Title

Eddy current–nulled convex optimized diffusion encoding (EN-CODE) for distortion-free diffusion tensor imaging with short echo times

Journal

Magnetic Resonance in Medicine, 79(2)

ISSN

0740-3194

Authors

Aliotta, Eric
Moulin, Kévin
Ennis, Daniel B

Publication Date

2018-02-01

DOI

10.1002/mrm.26709

Peer reviewed

FULL PAPER

Magnetic Resonance in Medicine 00:00–00 (2017)

Eddy Current–Nulled Convex Optimized Diffusion Encoding (EN-CODE) for Distortion-Free Diffusion Tensor Imaging With Short Echo Times

Eric Aliotta,[1,2] Kévin Moulin,[1] and Daniel B. Ennis[1,2,3]*

Purpose: To design and evaluate eddy current–nulled convex optimized diffusion encoding (EN-CODE) gradient waveforms for efficient diffusion tensor imaging (DTI) that is free of eddy current–induced image distortions.

Methods: The EN-CODE framework was used to generate diffusion-encoding waveforms that are eddy current–compensated. The EN-CODE DTI waveform was compared with the existing eddy current–nulled twice refocused spin echo (TRSE) sequence as well as monopolar (MONO) and non–eddy current–compensated CODE in terms of echo time (TE) and image distortions. Comparisons were made in simulations, phantom experiments, and neuro imaging in 10 healthy volunteers.

Results: The EN-CODE sequence achieved eddy current compensation with a significantly shorter TE than TRSE (78 versus 96 ms) and a slightly shorter TE than MONO (78 versus 80 ms). Intravoxel signal variance was lower in phantoms with EN-CODE than with MONO (13.6 ± 11.6 versus 37.4 ± 25.8) and not different from TRSE (15.1 ± 11.6), indicating good robustness to eddy current–induced image distortions. Mean fractional anisotropy values in brain edges were also significantly lower with EN-CODE than with MONO (0.16 ± 0.01 versus 0.24 ± 0.02, $P < 1 \times 10^{-5}$) and not different from TRSE (0.16 ± 0.01 versus 0.16 ± 0.01, $P =$ nonsignificant).

Conclusions: The EN-CODE sequence eliminated eddy current–induced image distortions in DTI with a TE comparable to MONO and substantially shorter than TRSE. **Magn Reson Med 000:000–000, 2017. © 2017 International Society for Magnetic Resonance in Medicine.**

Key words: diffusion; DTI; distortion; eddy currents

INTRODUCTION

Diffusion-weighted imaging (DWI) uses large amplitude gradient pulses to impart sensitivity to diffusion in the MRI signal amplitude. These same gradients, however, induce eddy currents within conductive hardware components in the MRI system, which generate additional magnetic fields. The use of active-gradient coil shielding (1–3), advanced gradient coil designs (4), and gradient pre-emphasis corrections (5,6) has reduced the magnitude and effect of eddy currents, but they can still lead to substantial image distortions with the large amplitude gradient pulses used in DWI. These image distortions are especially apparent in echo planar imaging (EPI)—the readout most commonly used in both DWI and diffusion tensor imaging (DTI)—which is particularly sensitive to magnetic field perturbations. Within a specific protocol, eddy current–induced image distortions are dependent on the direction and magnitude (ie, b-value) of the diffusion-encoding gradients, which leads to misregistration among different DWI and confounds diffusion tensor reconstruction if not carefully corrected for in postprocessing (7,8).

In addition to improved gradient hardware and postprocessing methods, modified pulse-sequence approaches are another solution strategy. For example, the twice-refocused spin-echo (TRSE) pulse sequence (9) significantly reduces eddy current–induced image distortions. The TRSE sequence balances the eddy currents produced by each diffusion-encoding gradient ramp by using a bipolar gradient encoding design and an additional refocusing pulse. Twice-refocused spin-echo is an effective technique for mitigating eddy current–induced distortions, but it significantly increases echo times (TEs) compared with conventional monopolar (MONO) encoding. This is particularly true for low to moderate b-values ($b \leq 1000$ s/mm^2) and long EPI readouts (≥ 50 ms, ie, high spatial resolution imaging). The use of two refocusing pulses also enhances sensitivity to B_1 imperfections and increases specific absorption rate deposition (10).

Recently, convex optimized diffusion encoding (CODE) was described as a framework for generating time-optimal (minimum TE) gradient waveforms for spin-echo EPI (SE-EPI) DWI (11). The CODE framework formulates the design of the diffusion-encoding gradient waveforms as a constrained (ie, gradient hardware limits, pulse sequence timing constraints, b-value, and gradient moment requirements) convex optimization problem. Consequently, CODE can efficiently determine the diffusion-encoding gradient waveform that optimally satisfies all requirements and produces the shortest TE.

In this work, the CODE framework was used to design eddy current–compensated diffusion-encoding gradient waveforms for DTI that is free of eddy current image distortions with a single refocusing pulse. To do so, an additional eddy current nulling constraint was incorporated into the CODE optimization framework. The resultant eddy current–nulled convex optimized diffusion

[1]Department of Radiological Sciences, University of California, Los Angeles, California, USA.

[2]Biomedical Physics Interdepartmental Program, University of California, Los Angeles, California, USA.

[3]Department of Bioengineering, University of California, Los Angeles, California, USA.

*Correspondence to: Daniel B. Ennis, Ph.D., Peter V. Ueberroth Building, Suite 1471, Room B, 10945 Le Conte Avenue, Los Angeles, CA 90095, USA. Tel: 1.310.206.0713; Fax: 1.310.825.5837; E-mail: DEnnis@mednet.ucla.edu

Received 4 December 2016; revised 25 February 2017; accepted 21 March 2017

DOI 10.1002/mrm.26709

Published online 00 Month 2017 in Wiley Online Library (wileyonlinelibrary.com).

encoding (EN-CODE) gradient waveforms shorten the TE compared with both TRSE and MONO DTI, particularly for low b-values and high spatial resolution imaging. The EN-CODE sequence was evaluated using eddy current simulations as well as imaging in both phantoms and healthy volunteers.

THEORY

CODE Optimization Framework

The previously reported CODE framework uses convex optimization to design diffusion-encoding gradient waveforms that minimize TE in SE-EPI DWI for a given b-value with no explicit constraint on gradient waveform shape or symmetry (11). Minimum TE waveforms are achieved by first maximizing the b-value for any particular sequence timing, which is given by

$$b = \gamma^2 \int_0^{T_{Diff}} F(t)^2 dt \quad [1]$$

where b is the b-value; γ is the gyromagnetic ratio of ^{1}H; T_{Diff} is the time corresponding to the end of diffusion encoding, and

$$F(t) = \int_0^t G(\tau) d\tau \quad [2]$$

where the time $t = 0$ corresponds with the center of the excitation pulse.

However, because the b-value (Eq. [1]) is a convex and nonunique function of G(t), it does not contain a single maximum that can be determined through convex optimization. To facilitate convex optimization, the objective function can be reformulated by defining the function, β, as

$$\beta = \int_o^{T_{Diff}} F(t) dt \quad [3]$$

The magnitude of β corresponds directly with the b-value, but it is a concave functional of G(t) (ie, its second variation is negative definite (12)); thus, it contains a unique maximum that can be determined using convex optimization. Consequently, the gradient waveform G(t) that maximizes β (and thus the b-value) can be determined using the following objective function:

$$G(t) = \arg\max_G \beta(G) \quad [4]$$

G(t) is defined discretely and arbitrarily on $t = m \bullet dt$, in which *m* is an integer number of gradient time points, and *dt* is the temporal discretization of the optimization.

Optimization Constraints

In addition to maximizing the b-value, CODE diffusion-encoding gradient waveforms must also be achievable on an MRI system. Therefore, the CODE optimization includes three constraints: (i) pulse sequence timing constraints to ensure that gradients are off during periods of radiofrequency activity and during readout; (ii) gradient moment constraints to ensure that the total gradient area (ie, M_0) is zero and that higher-order gradient moments (M_1, M_2) for motion-compensated diffusion encoding are zero as needed (M_1 and M_2 were not nulled in the present study); and (iii) hardware constraints to limit the gradient waveform design to operate within gradient amplitude and slew-rate limits. The EN-CODE sequence adds a fourth constraint on the diffusion-encoding gradient waveform for eddy current nulling.

Eddy Current Model

Eddy currents are generated within various conductive MRI hardware components during the application of time-varying gradient pulses. Eddy currents predominantly exhibit exponential decay over time and can be modeled as a resistive-inductive circuit. The eddy currents generated during equivalent gradient ramp-up and ramp-down intervals (eg, in a trapezoidal gradient waveform) are equal in magnitude and opposite in direction. Exponential decay of the eddy currents generated at earlier time points, however, leads to imperfect cancellation and a nonzero superposition of the eddy current–induced magnetic fields (B_{EC}). These magnetic fields can persist during the EPI readout and result in deviations from the target *k*-space trajectory and substantial image distortions. By modeling the induced eddy currents with a resistive-inductive circuit B_{EC} from an arbitrary gradient waveform, G(t) can be described as follows (13):

$$B_{EC}(t) = \sum_i w(\lambda_i)\left(\frac{dG}{dt} * e^{-\frac{t}{\lambda_i}}\right) \quad [5]$$

where * is the convolution operator; λ_i are the time constants of eddy current decay; and *w* is a system-dependent scaling factor for each λ_i. Previous approaches have effectively eliminated eddy current–induced image distortions by compensating for a single λ (9,14). Considering only a single λ reduces the problem to

$$B_{EC}(\lambda, t) = w(\lambda)\frac{dG}{dt} * e^{-\frac{t}{\lambda}} \quad [6]$$

In general, *w* is scanner-dependent scalar value, but it is not necessary to know the value to null eddy currents for any single λ, if the convolution term can be minimized at a specific time. Therefore, a new function is defined that is proportional to B_{EC}, but independent of w:

$$\varepsilon(\lambda, t) = \frac{dG}{dt} * e^{-\frac{t}{\lambda}} \quad [7]$$

An eddy current nulling constraint can then be defined using Equation [7] as follows:

$$\varepsilon(\lambda_{null}, T_{Diff}) = 0 \quad [8]$$

where λ_{null} is the target decay constant to be nulled. Importantly, nulling eddy currents at T_{Diff} ensures that eddy current contributions from the diffusion-encoding gradient waveform are zero for all $t \geq T_{Diff}$.

Comparing the magnitude of eddy current–induced artifacts between two different pulse sequences is

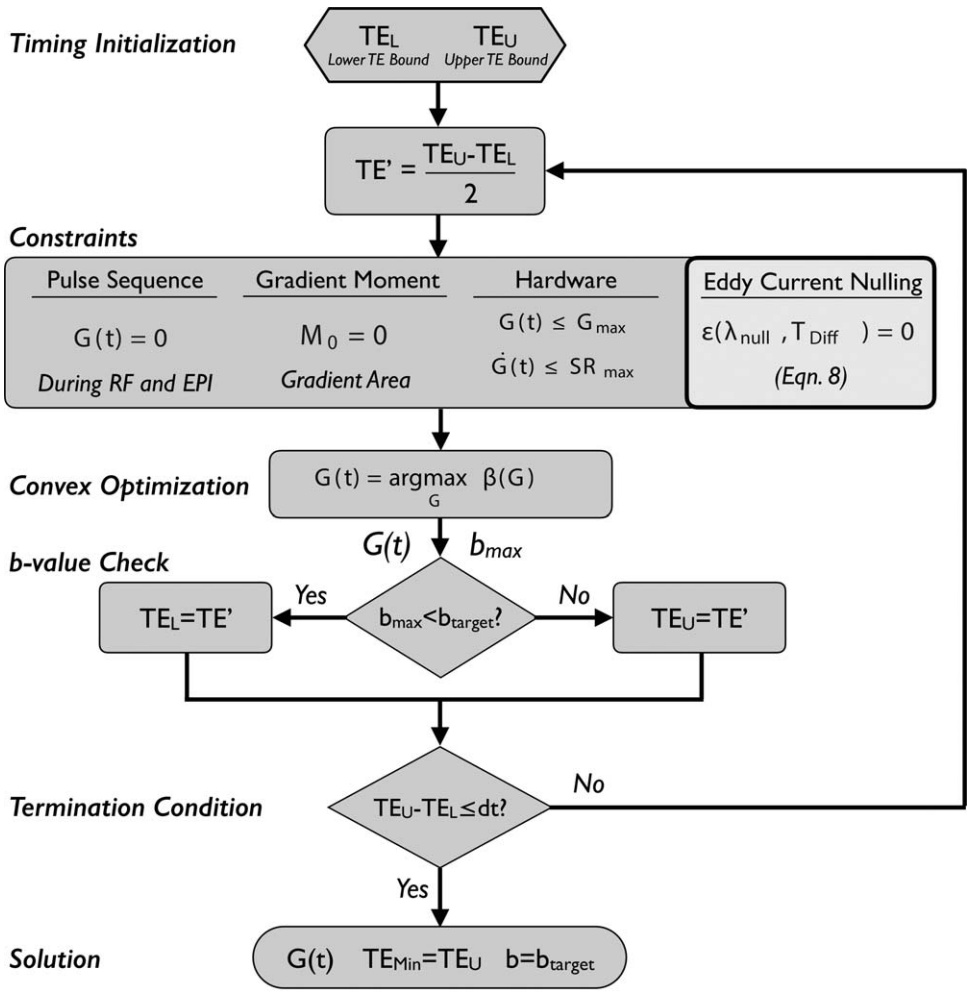

FIG. 1. The EN-CODE gradient optimization algorithm. The time-optimal solution is determined by finding the minimum TE for which a diffusion-encoding gradient waveform that is both consistent with all constraints and achieves the target b-value (b_{target}) exists. Successive binary searches divide the TE search space with each call of the convex solver. The function β (Eq. [4]) is directly related to the b-value (ie, maximizing β also maximized the b-value) and is compatible with convex optimization. The EN-CODE algorithm is equivalent to the previously described CODE algorithm with the added eddy current nulling constraint.

typically an empirical exercise. Note, however, that Equation [7] can also be used to define the eddy current characteristics of any diffusion-encoding gradient waveform, which we term the "eddy current spectrum." By calculating ε(λ,t) over a range of λ, and at the end of diffusion encoding (T_{Diff}), the eddy current spectrum can be compared among different diffusion-encoding gradient waveforms. Importantly, because *w* is not included in this formulation, the eddy current spectrum is system-invariant.

Solution Strategy

The time-optimal EN-CODE gradient waveforms are determined by finding the minimum TE for which a gradient waveform exists that is consistent with all constraints and reaches the desired b-value. This is efficiently accomplished using a binary search through a TE search space with each iteration of Equation [4] (11,15) (Fig. 1). Upper and lower limits on TE (TE_U and TE_L) are first defined to initialize the optimization. TE_U is defined by the TE of MONO plus 20 ms, which was a suitable upper bound in all cases examined. TE_L is defined by the TE of a spin-echo sequence without diffusion-encoding gradients, which has a minimum TE of $T_{180} + 2T_\varepsilon$, in which T_ε is the duration of the EPI readout before the spin echo (exactly half of the readout time for full-Fourier imaging) and T_{180} is the refocusing pulse duration.

METHODS

Simulations

The EN-CODE diffusion-encoding gradient waveforms were designed with a range of individual λ_{null} (10–100 ms, $\Delta\lambda_{null} = 10$ ms) using the algorithm shown in Figure 1. This range of λ_{null} values was chosen to match the time scale of the DWI pulse sequence and corresponds with values that have been previously shown to be relevant on a clinical MRI system (9,10,14). The simulated pulse-sequence parameters were $b = 1000$ s/mm^2, bandwidth = 1852 Hz/pixel (0.6 ms echo spacing), $T_\varepsilon = 27.5$ ms and $T_{180} = 5.2$ ms, corresponding with a neuro DTI protocol with 1.7-mm in-plane resolution and a 300 x

Table 1
The DWI/DTI Protocol Details for Both Phantom and In Vivo Imaging

	FOV (mm)	Resolution (mm)	b-value (s/mm^2)	TR (ms)	TE (ms)	Other
MONO	300 × 300	1.7 × 1.7 × 5.0	1000	2300	80	2× GRAPPA 5 averages 15 slices Band width = 1852 Hz/px
CODE					71	
TRSE					96	
EN-CODE					76–78	

300 mm field of view (FOV) that was subsequently used for phantom and in vivo imaging. Hardware constraints were defined for a 3 Tesla (T) MRI scanner with high-performance gradients ($G_{max} = 80$ mT/m and $SR_{max} = 200$ T/m/s), but with G_{max} limited to 76 mT/m and SR_{max} limited to 50 T/m/s to limit peripheral nerve stimulation during diffusion encoding. All optimizations were performed in MATLAB (The MathWorks, Natick, MA) using the CPLEX linear solver (IBM Corp, Armonk, NY) and the YALMIP toolbox (16) with a time step $dt = 100\,\mu s$ that maintained EN-CODE gradient waveform computation times to less than 5 min without notably affecting the minimum possible TE.

Analogous TRSE diffusion-encoding gradient waveforms were also designed using the same pulse-sequence parameters and hardware constraints and with the same λ_{null} values used for EN-CODE. Conventional MONO waveforms and non–eddy current–compensated CODE waveforms were also designed. Eddy current spectra were then simulated for each diffusion-encoding gradient waveform using Equation [7] for a range of λ (0 to 100 ms, $\Delta\lambda = 1$ ms) and T_{Diff} matched to each sequence.

Echo time differences between EN-CODE and alternative diffusion-encoding methods were also evaluated. Minimum TEs were compared over a range of b-values (200 to 2000 s/mm^2) and T_ε (10–60 ms) (corresponding to approximately 0.5 to 3.0 mm isotropic in-plane resolution, with full-Fourier symmetric *k*-space coverage) using (i) TRSE with $\lambda_{null} = 80$ ms; (ii) EN-CODE with $\lambda_{null} = 80$ ms; and (iii) MONO. A λ_{null} of 80 ms was used based on the findings of the phantom imaging experiments shown subsequently.

Phantom Imaging

Phantom experiments were performed to evaluate eddy current–induced image distortions among diffusion-encoding methods and to determine the optimal λ_{null} for our system. A phantom containing 50-mL conical tubes (diameter of 5.5 cm) of water submerged in a susceptibility-matched fluid with a negligible MRI signal (Fomblin, Solvay Solexis, West Deptford, NJ) was imaged using a 3T scanner (Prisma, Siemens, Erlangen, Germany). The DWIs were acquired with $b = 1000$ s/mm^2 along six diffusion-encoding directions ($\pm x, \pm y, \pm z$), 1.7 x 1.7 x 5 mm spatial resolution ($T_\varepsilon = 27.5$ ms), 15 interleaved slices, parallel imaging acceleration factor of two with GRAPPA (17), five averages to improve signal-to-noise ratio, and repetition time (TR) = 2300 ms (Table 1). All acquisition parameters were matched, except TE, for all diffusion-encoding schemes: (i) MONO (TE = 80 ms); (ii) CODE (TE = 71 ms); (iii) TRSE with $\lambda_{null} = 20$–100 ms (TE = 96 ms); and (iv) EN-CODE with $\lambda_{null} = 10$–100 ms (TE = 76–78 ms). A $\Delta\lambda_{null}$ of 10 ms was used for TRSE and EN-CODE. Note that $\lambda_{null} = 10$ ms was not achievable for TRSE with this protocol, because of timing constraints imposed by this particular T_ε. The EN-CODE waveforms were calculated offline as described previously and then implemented on the scanner.

Eddy current–induced image distortions were evaluated for each diffusion-encoding waveform by measuring the pixel-wise coefficient of variation (CoV) across the three acquired directions. The mean global CoV (CoV_{Global}) was then calculated within all water voxels (masked to exclude the very low Fomblin signal in the $b = 0$ images) as well as edge voxels (CoV_{Edge}) at water-Fomblin interfaces. Masking was performed using magnitude thresholding and built-in binary image operations in MATLAB.

The optimal λ_{null} were determined for EN-CODE and TRSE by comparing the mean CoV_{Edge} from the acquisitions with each of the 10 λ_{null} values. The λ_{null} that led to the minimum CoV_{Edge} was then used for in vivo imaging.

Apparent diffusion coefficient (ADC) maps were also reconstructed from each DWI set, and the mean global ADC values were measured within all water voxels.

In Vivo Imaging

Neuro DTI were acquired in healthy volunteers ($n = 10$) to further compare the four diffusion-encoding protocols. Four DTI sets were acquired: (i) MONO; (ii) CODE; (iii) TRSE with $\lambda_{null} = 80$ ms; and (iv) EN-CODE with $\lambda_{null} = 80$ms. A λ_{null} of 80 ms was chosen for TRSE and EN-CODE based on the phantom results. The in vivo protocol was identical to the phantom study, but with 20 diffusion-encoding gradient directions to facilitate tensor reconstruction (Table 1).

Images were reconstructed using the manufacturer-provided pipeline, and no additional image registration or distortion correction was performed to correct for eddy current–induced image distortion before offline tensor reconstruction from each DTI set. Fractional anisotropy (FA) maps were then generated offline from the diffusion tensors. The mean whole-brain global FA (FA_{Global}) was measured for each diffusion-encoding protocol within a manually drawn whole-brain mask on the $b = 0$ images and in the outermost single-pixel layer from the global mask (FA_{Edge}). To visualize differences in eddy current–induced image distortion, FA-weighted color maps of the diffusion tensor primary eigenvector (red, green, and blue mapped to *x, y*, and *z*) were generated for each subject (18). A supplemental video is also available online.

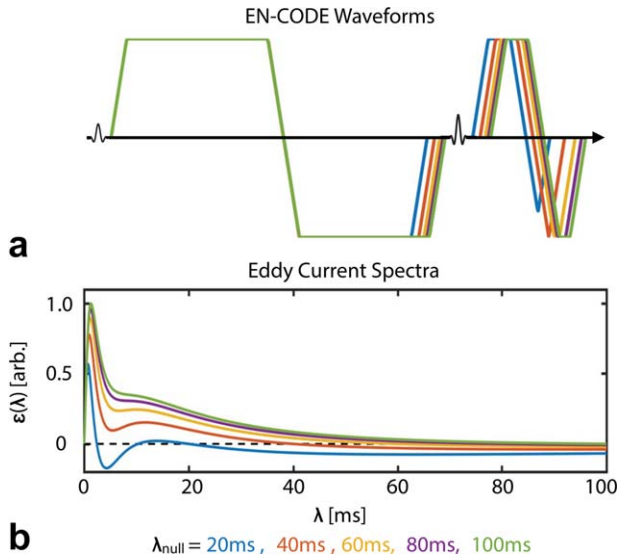

FIG. 2. (**a**) The EN-CODE diffusion-encoding gradient waveforms designed for $\lambda_{NULL} = 20$, 40, 60, 80, and 100 ms. Although EN-CODE does not impose any specific gradient shape, the resultant waveforms contain only trapezoidal and triangular pulses. (**b**) The resultant eddy current spectra for each of the waveforms shown in (**a**). Each waveform nulls the eddy currents with $\lambda = \lambda_{null}$. $\lambda_{null} = 80$ ms empirically produced the smallest eddy current–induced image distortion on our system and was used for all in vivo imaging. Note that while the location of the refocusing radiofrequency pulse varies slightly between waveforms in (**a**), the position shown is approximated to improve visibility.

All values are reported as mean ± 1 SD, and comparisons were made using paired t-tests, in which P values < 0.05 were deemed statistically significant.

RESULTS

Simulations

Figure 2 shows EN-CODE gradient waveforms generated for a range of λ_{null} values and the corresponding eddy current spectra, normalized to the largest peak. Each EN-CODE gradient waveform nulled the eddy currents for each specified λ_{null}.

Pulse sequence diagrams for MONO, CODE, TRSE with $\lambda_{null} = 80$ ms, and EN-CODE with $\lambda_{null} = 80$ ms are shown in Figure 3. Each was used for both phantom and in vivo imaging. The TRSE had the longest TE (96 ms), which was reduced to 80 ms with MONO, further reduced to 78 ms with EN-CODE, and minimized to 71 ms with CODE. The eddy current spectra for each sequence are shown in Figure 4. The MONO encoding demonstrated the largest residual eddy currents across all time constants (λ), whereas CODE notably reduced the eddy currents at all λ while minimizing TE, compared with the other three methods. The TRSE and EN-CODE sequences demonstrated even greater eddy current reductions, particularly for $\lambda > 20$ ms.

The minimum TE for TRSE ($\lambda_{null} = 80$ ms), EN-CODE ($\lambda_{null} = 80$ ms), and MONO over a range of b-values and T_ε, as well as TE differences between sequences, are shown in Figure 5. The EN-CODE sequence had a shorter TE than TRSE for 78% of the examined cases ($TE_{TRSE} - TE_{EN\text{-}CODE} = 20.8 \pm 18.8$ ms) and a shorter TE than MONO in 65% of the cases ($TE_{MONO} - TE_{EN\text{-}CODE} = 3.1 \pm 12.7$ ms) while conferring eddy current insensitivity. The EN-CODE sequence had a longer TE than MONO for short EPI readouts ($T_\varepsilon < 25$ ms) at b-values above 500 s/mm^2 and a longer TE than TRSE for short EPI readouts ($T_\varepsilon < 30$ ms) at all b-values. For $T_\varepsilon \geq 30$ ms, EN-CODE had a shorter TE than MONO and TRSE for all b-values. The choice of λ_{null} had only a small effect on the TE for EN-CODE (the maximum TE difference between λ_{null} values was 2 ms) and had no effect on TE for TRSE.

Phantom Imaging

CoV_{Edge} was plotted for MONO and CODE, and for TRSE and EN-CODE, as a function of λ_{null} (Fig. 6). CoV_{Edge} was greatest for MONO ($CoV_{Edge} = 37.4 \pm 25.8\%$) and reduced by 39% with CODE ($CoV_{Edge} = 22.8 \pm 18.0\%$). The minimum CoV_{Edge} for EN-CODE was achieved with $\lambda_{null} = 80$ ms ($CoV_{Edge} = 13.6 \pm 11.6\%$), which reduced CoV_{Edge} by

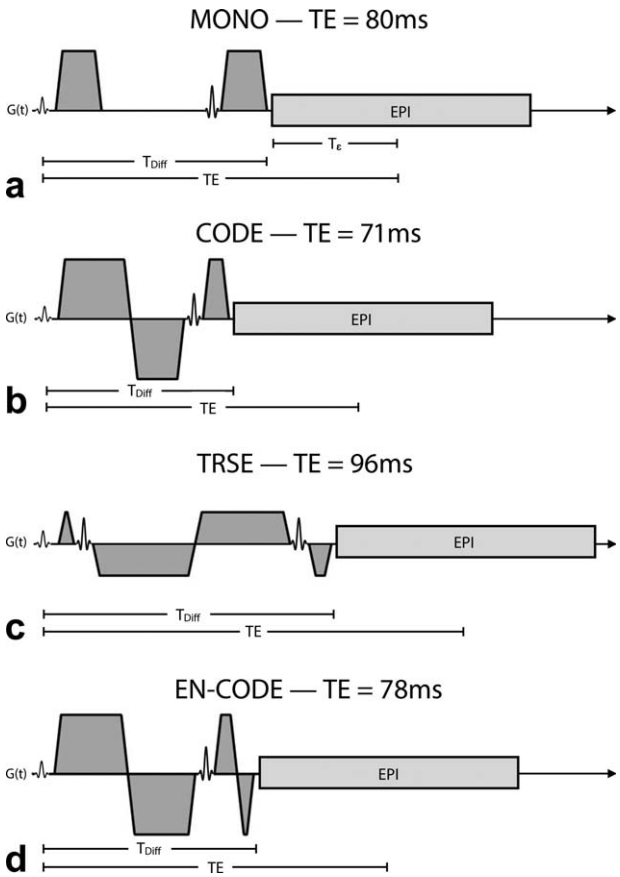

FIG. 3. Pulse sequence diagrams for b = 1000 s/mm^2 with MONO (**a**), CODE (**b**), TRSE (**c**), and EN-CODE (**d**) diffusion encoding. The EPI time-to-echo, T_ε, was 27.5 ms, which agrees with the 1.7-mm in-plane spatial resolution (FOV = 300 × 300 mm) for all four sequences. The MONO and CODE frameworks are both susceptible to eddy current distortions, whereas TRSE and EN-CODE are eddy current–compensated. The EN-CODE sequence accomplishes eddy current nulling with a slight TE decrease compared with MONO, whereas TRSE requires a significant TE increase compared with MONO.

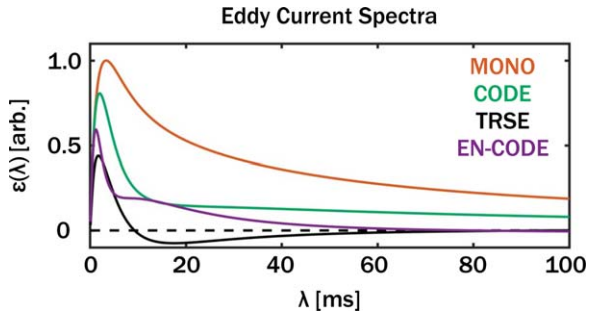

FIG. 4. Simulated eddy current spectra at the end of diffusion encoding (T_{Diff}) for a range of eddy current decay time constants (λ) for each sequence are shown in Figure 3. Spectra are normalized by the peak of the MONO spectrum. The MONO framework generates the largest residual eddy currents for all values of λ. The CODE framework notably reduces eddy currents while minimizing TE, whereas TRSE and EN-CODE lead to large reductions for λ greater than 20 ms and an eddy current null point at the prescribed $\lambda_{NULL} = 80$ ms.

64% compared with MONO, and was used for subsequent in vivo imaging. The TRSE sequence demonstrated minimal variation with the choice of λ_{null} (CoV_{Edge} differences were $\leq 0.9\%$ between λ_{null} values), so $\lambda_{null} = 80$ ms was also used for TRSE in vivo ($CoV_{Edge} = 15.1 \pm 11.6\%$).

CoV maps for MONO, CODE, TRSE ($\lambda_{null} = 80$ ms) and EN-CODE ($\lambda_{null} = 80$ms) in a single slice are shown in Figure 7a. The CoV was high for MONO near phantom edges (water-Fomblin interfaces), indicating eddy current–induced misregistration between images with different diffusion-encoding directions. This effect was mitigated with CODE and substantially reduced with TRSE and EN-CODE, as shown in the CoV_{Global} and CoV_{Edge} values plotted in Figure 7b.

No significant differences were observed in mean ADC values from any of the sequences. The MONO ADC was $2.1 \pm 0.3\,mm^2/ms$, the CODE ADC was $2.1 \pm 0.25\,mm^2/ms$, the TRSE ($\lambda_{null} = 80$ ms), the ADC was $2.1 \pm 0.25\,mm^2/ms$, and the EN-CODE ($\lambda_{null} = 80$ ms) ADC was $2.1 \pm 0.22\,mm^2/ms$.

In Vivo Imaging

A representative neuro DTI example is shown in Figure 8. The apparent SNR of the DWI from TRSE was lower compared with the other sequences, because of the longer TE (Fig. 8a) and the second refocusing pulse. Eddy current distortion between diffusion-encoding directions in MONO and CODE led to regions of notably elevated FA near brain edges (Fig. 8b and 8c) that were largely eliminated with TRSE and EN-CODE. Differences in eddy current–induced image distortions among techniques are also demonstrated

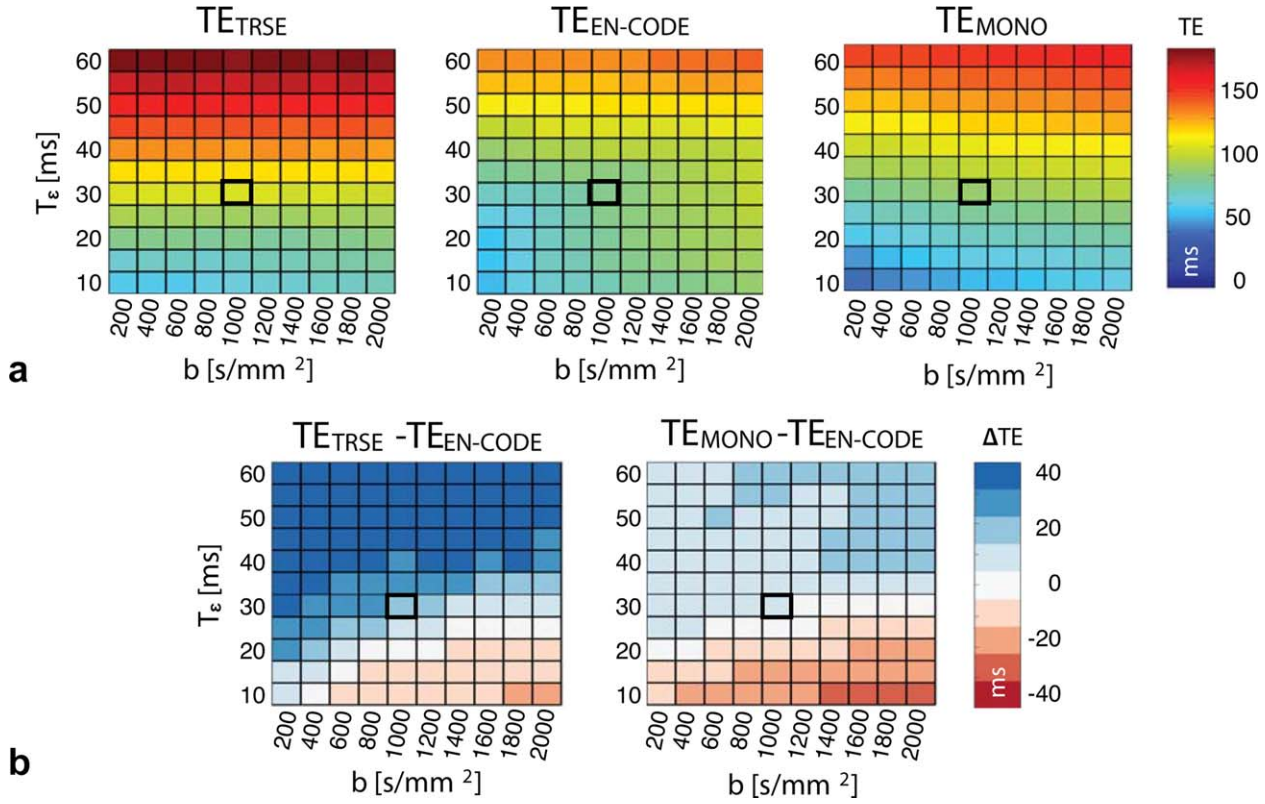

FIG. 5. (**a**) The minimum TE as a function of b-value and EPI time-to-echo, T_ε, for TRSE, EN-CODE, and MONO diffusion encoding. (**b**) Echo time differences between TRSE and EN-CODE (left) as well as between MONO and EN-CODE (right). Positive values (blue) indicate EN-CODE has a shorter TE, whereas negative values (red) indicate EN-CODE has a longer TE. The EN-CODE sequence had shorter TEs than TRSE in 78% of instances, and shorter TEs than MONO in 65% of instances. The black square indicates the parameters used for phantom and in vivo imaging in this study, and are plotted in Figure 3. The upper row ($T_\varepsilon = 60$ ms) corresponds to a DTI protocol with approximate 0.5-mm in-plane spatial resolution with a full-Fourier readout; the lower row ($T_\varepsilon = 10$ ms) corresponds to an approximate 3.0-mm resolution.

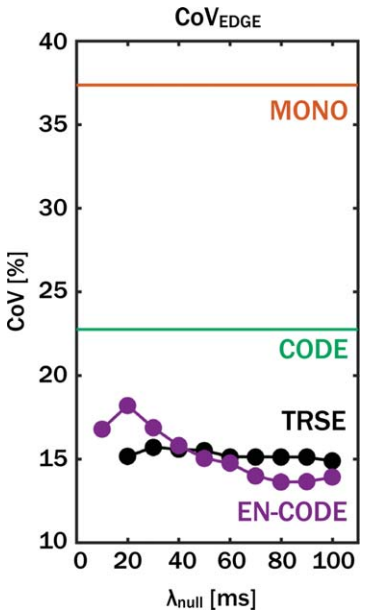

FIG. 6. Diffusion tensor imaging distortion, quantified by the mean coefficient of variation across diffusion-encoding directions within phantom edges (CoV_{Edge}), for each of the pulse sequences examined. Image reconstruction was performed using only the vendor-provided pipeline, and no eddy current image distortion correction was performed. The MONO framework was the worst ($CoV_{Edge} = 37.4 \pm 25.8$), whereas CODE performed slightly better ($CoV_{Edge} = 22.8 \pm 18.0$). For MONO and CODE, these results are independent of λ_{null}. The TRSE and EN-CODE sequences substantially reduced image distortion for all choices of λ_{null}. The CoV_{Edge} was minimized for EN-CODE with $\lambda_{null} = 80$ ms ($CoV_{Edge} = 13.6 \pm 11.6$), which was used for subsequent in vivo imaging. The choice of λ_{null} had little effect on distortion for TRSE, so $\lambda_{null} = 80$ms ($CoV_{Edge} = 15.1 \pm 11.6$) was also used for TRSE in vivo.

in Supporting Video S1, which includes a second example with a movie cycling through all diffusion-encoding directions.

Global FA analysis is shown in Figure 9. The FA was reduced with CODE compared with MONO ($FA_{Global} = 0.24 \pm 0.01$ versus 0.25 ± 0.01, $P = 0.02$; $FA_{Edge} = 0.21 \pm 0.02$ versus 0.24 ± 0.02, $P = 3 \times 10^{-4}$). The FA was further reduced with EN-CODE compared with MONO ($FA_{Global} = 0.24 \pm 0.01$ versus 0.25 ± 0.01, $P = 1.5 \times 10^{-4}$; $FA_{Edge} = 0.16 \pm 0.01$ versus 0.24 ± 0.02, $P < 1 \times 10^{-5}$). Similar FA reductions were observed with TRSE compared with MONO ($FA_{Global} = 0.23 \pm 0.01$ versus 0.25 ± 0.01, $P = 1 \times 10^{-5}$; $FA_{Edge} = 0.16 \pm 0.01$ versus 0.24 ± 0.02, $P < 1 \times 10^{-5}$). There was no significant difference between TRSE and EN-CODE for either FA_{Global} or FA_{Edge}.

DISCUSSION

The results of the simulations, phantom imaging, and in vivo imaging all indicate that EN-CODE achieves a significant reduction of eddy current distortions compared with MONO. In simulations, EN-CODE reduced the TE compared with MONO and TRSE for a wide range of imaging and diffusion-weighting parameters, only failing to do so for very short (ie, low-resolution) EPI readouts. Symmetric, full-Fourier k-space coverage was used in this work, but partial Fourier imaging can be used to substantially shorten T_ε and thereby reduce TE, particularly for TRSE and, to a lesser extent MONO, which would reduce or eliminate the TE reduction of EN-CODE. However, the use of partial Fourier leads to an increase in bulk-motion sensitivity (19), the potential for additional signal attenuation from eddy currents (20), a broader point-spread function, and lower signal-to-noise ratio. The EN-CODE sequence can be used to shorten TE without the drawbacks of partial Fourier imaging. For the protocol used in this study (1.7-mm in-plane resolution, $b = 1000$ s/mm^2), a partial Fourier factor of 6/8 (ie, $T_\varepsilon = 20.6$ ms) results in a TE of 78 ms for TRSE, which is equivalent to full-Fourier EN-CODE.

Although EN-CODE reduced the TE compared with TRSE and MONO for a wide range of acquisition parameters, it led to longer TEs for cases with high b-values and very short (ie, low spatial resolution, partial Fourier) EPI readouts. In these cases, the temporal footprint of the readout within the TE is reduced, which improves the efficiency of nonoptimized waveforms. Therefore, TRSE may be a better choice for these applications. The EN-CODE framework is compatible with a TRSE-like double-echo sequence that, when combined, may also confer TE reductions. However, this has not been evaluated in the present study.

Eddy current distortions in EN-CODE were more sensitive to the choice of λ_{null} than TRSE. This may be because of the substantially lower gradient amplitudes used in TRSE than in EN-CODE (gradient amplitude was 46 mT/m for TRSE versus 76 mT/m for EN-CODE). The use of two refocusing pulses in TRSE causes the minimum TE to be especially dictated by T_ε rather than b-value (as shown by the flat TRSE TE distribution in Fig.

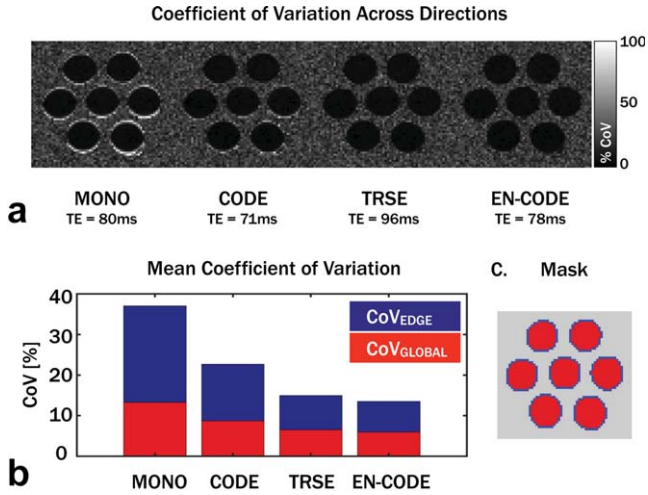

FIG. 7. (**a**) Coefficient of variation maps calculated across all diffusion-encoding directions for each technique. (**b**) Mean CoV values within all cylinders, CoV_{Global} (red), and within edge voxels only, CoV_{Edge} (blue). High CoV indicates large differences in signal intensity between diffusion directions, which is indicative of eddy current–induced image distortions. The CoV was largest with the MONO sequence, reduced with CODE, and further reduced with TRSE and EN-CODE, especially for edge voxels. (**c**) The segmentation used for global analysis.

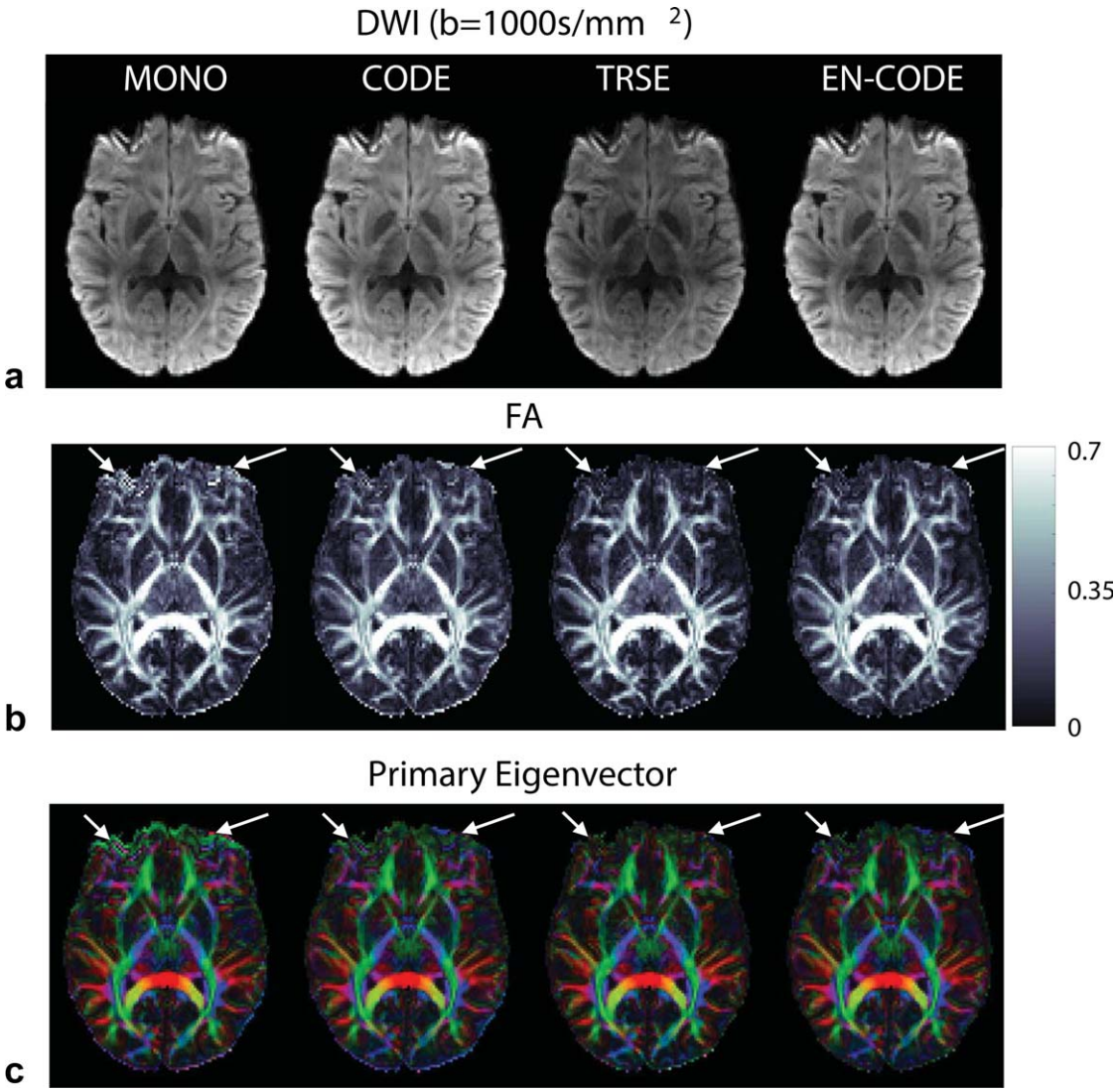

FIG. 8. (**a**) Diffusion-weighted images from each technique with matched window and level, (**b**) reconstructed FA maps, and (**C**) FA-weighted primary eigenvector maps in which the *x, y*, and *z* vector components are mapped to red, green and blue, respectively. The MONO diffusion encoding leads to substantial eddy current image distortions, which lead to regions of artificially high FA (white arrows). These were reduced with CODE and further reduced with TRSE and EN-CODE. The EN-CODE sequence, however, had a shorter TE than TRSE (78 versus 96 ms), which led to higher apparent signal-to-noise ratio in (**a**).

5), which also indicates that higher b-values could have been accomplished without increasing TE by increasing gradient amplitude. This also led to lower slew rates for TRSE (30 T/m/s), because ramp times were fixed for all diffusion-encoding gradients in our vendor-provided implementation of TRSE. Further optimization could have therefore led to a slightly shorter TE for TRSE. However, even with the higher gradient amplitudes and higher slew rates, EN-CODE ($\lambda_{null} = 80$ ms) achieved equivalent eddy current–nulling performance to TRSE ($\lambda_{null} = 80$ ms).

The relatively flat behavior of EN-CODE for $\lambda_{null} \geq 50$ ms indicates that the technique is unlikely to be sensitive to slight variations in hardware between scanners or to the presence of multiple eddy current decay times. This behavior is also consistent with the smooth eddy current spectra for EN-CODE, as shown in Figure 2. Further distortion reductions may be achievable by nulling multiple values of λ_{null} as previously shown in a double-echo sequence (10), albeit with likely TE increases.

The in vivo neuro DTI results demonstrate that EN-CODE improves diffusion tensor reconstruction without the need for postprocessing eddy current corrections. Although numerous image processing corrections exist that improve DTI reconstruction in the presence of eddy current distortions (8,20,21), an eddy current–nulled diffusion-encoding approach avoids the added complexity and potential for errors (22), and EN-CODE achieves this with no penalty, compared with MONO, over a wide range of acquisition parameters.

It is possible that subject motion between diffusion-encoding directions could have contributed to the observed artifacts near the edges of the brain. However, the consistency of our findings across 10 subjects indicates that eddy

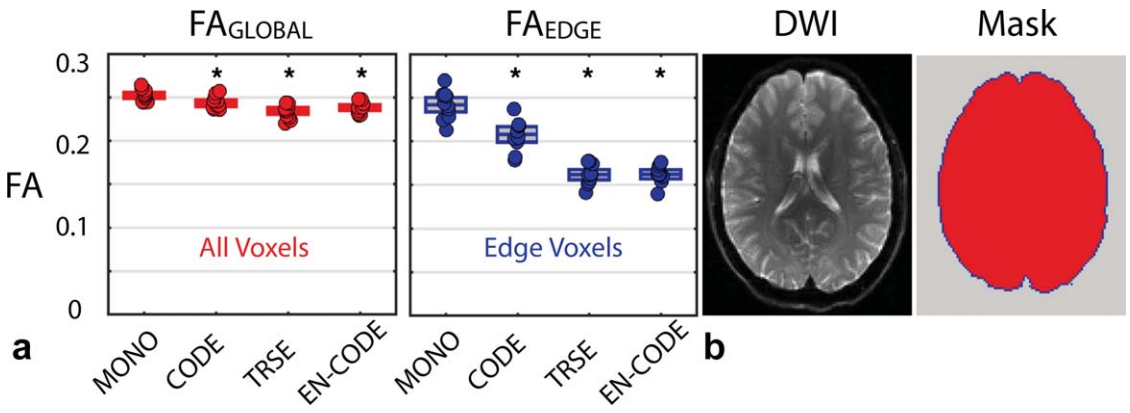

FIG. 9. (**a**) Mean global FA values measured in all brain voxels, FA_{Global} (red), and voxels along brain edges, FA_{Edge} (blue). * indicates significant differences from MONO ($P < 0.05$). (**b**) Example DWI and mask used for FA_{Global} and FA_{Edge} analysis. Notably, FA_{Edge} was highest with MONO, decreased with CODE, and decreased further with both TRSE and EN-CODE. This indicates that CODE reduces eddy current distortions compared with MONO and that both TRSE and EN-CODE further reduce them. Trends were equivalent for FA_{Global} and FA_{Edge}, but changes were exaggerated in edge voxels, where distortions have a larger effect on the diffusion tensor.

current–induced image distortions were the predominant cause of distortion in the MONO and CODE sequences.

Although it was not evaluated in this work, the tripolar approach for eddy current nulling previously described by Finsterbusch (14) also reduced the TE compared with TRSE in many scenarios, and used only a single refocusing pulse. The EN-CODE sequence has similar benefits to this approach, but has the added flexibility of optimally conforming to any set of sequence parameters. Furthermore, the tripolar approach uses a gap between gradient lobes to accomplish eddy current nulling, which leads to suboptimal diffusion-encoding efficiency, which extends the TE.

The EN-CODE gradients are not symmetric about the refocusing pulse; therefore, concomitant magnetic field corrections are needed to avoid significant image artifacts. A previously described linear correction was used in this work (11,23), and no residual effects were observed. This approach is used widely for TRSE and was also used for CODE in this work.

Also noteworthy is that CODE, which does not explicitly account for eddy currents, improved eddy current distortions compared with MONO, while substantially reducing the TE. The CODE sequence has previously been shown to reduce TE compared with MONO for a wide range of b-values and EPI durations (11), indicating that the CODE gradient design is both time optimal and more robust to eddy current–induced image distortion than MONO. However, both phantom and in vivo imaging showed that some residual eddy current effects were still present in CODE.

CONCLUSIONS

The EN-CODE sequence reduces eddy current–induced image distortions in DTI by incorporating eddy current compensation in the previously described CODE optimization framework. The EN-CODE framework also has a shorter TE compared with MONO and TRSE over a wide range of acquisition parameters.

ACKNOWLEDGEMENTS

The authors are grateful for research support from the Department of Radiological Sciences at UCLA and AHA 16PRE27380023 to EA.

REFERENCES

1. Mansfield P, Chapman B. Active magnetic screening of coils for static and time-dependent magnetic-field generation in NMR imaging. J Phys E Sci Instr 1986;19:540–545.
2. Mansfield P, Chapman B. Active magnetic screening of gradient coils in NMR imaging. J Magn Reson 1986;66:573–576.
3. Mansfield P, Chapman B. Multishield active magnetic screening of coil structures in NMR. J Magn Reson 1987;72:211–223.
4. Trakic A, Liu F, Lopez HS, Wang H, Crozier S. Longitudinal gradient coil optimization in the presence of transient eddy currents. Magn Reson Med 2007;57:1119–1130.
5. Jensen DJ, Brey WW, Delayre JL, Narayana PA. Reduction of pulsed gradient settling time in the superconducting magnet of a magnetic resonance instrument. Med Phys 1987;14:859–862.
6. Boesch C, Gruetter R, Martin E. Temporal and spatial analysis of fields generated by eddy currents in superconducting magnets: optimization of corrections and quantitative characterization of magnet/gradient systems. Magn Reson Med 1991;20:268–284.
7. Koch M, Norris DG. An assessment of eddy current sensitivity and correction in single-shot diffusion-weighted imaging. Phys Med Biol 2000;45:3821–3832.
8. Rohde GK, Barnett AS, Basser PJ, Marenco S, Pierpaoli C. Comprehensive approach for correction of motion and distortion in diffusion-weighted MRI. Magn Reson Med 2004;51:103–114.
9. Reese TG, Heid O, Weisskoff RM, Wedeen VJ. Reduction of eddy-current-induced distortion in diffusion MRI using a twice-refocused spin echo. Magn Reson Med 2003;49:177–182.
10. Finsterbusch J. Double-spin-echo diffusion weighting with a modified eddy current adjustment. Magn Reson Imaging 2010;28:434–440.
11. Aliotta E, Wu HH, Ennis DB. Convex optimized diffusion encoding (CODE) gradient waveforms for minimum echo time and bulk motion compensated diffusion weighted MRI. Magn Reson Med 2017;77:717–729.
12. Gel'fand IM, Fomin SV. Calculus of variations. Revised English edition. Englewood Cliffs, NJ: Prentice-Hall; 1963.
13. Bernstein MA, King KF, Zhou ZJ. Handbook of MRI pulse sequences. Amsterdam; Boston: Academic Press; 2004. pp xxii,1017.
14. Finsterbusch J. Eddy-current compensated diffusion weighting with a single refocusing RF pulse. Magn Reson Med 2009;61:748–754.
15. Hargreaves BA, Nishimura DG, Conolly SM. Time-optimal multidimensional gradient waveform design for rapid imaging. Magn Reson Med 2004;51:81–92.

16. Lofberg J. Automatic robust convex programming. Optim Methods Softw 2012;27:115–129.
17. Griswold MA, Jakob PM, Heidemann RM, et al. Generalized autocalibrating partially parallel acquisitions (GRAPPA). Magn Reson Med 2002;47:1202–1210.
18. Pajevic S, Pierpaoli C. Color schemes to represent the orientation of anisotropic tissues from diffusion tensor data: application to white matter fiber tract mapping in the human brain. Magn Reson Med 1999;42:526–540.
19. Storey P, Frigo FJ, Hinks RS, et al. Partial k-space reconstruction in single-shot diffusion-weighted echo-planar imaging. Magn Reson Med 2007;57:614–619.
20. Truong TK, Song AW, Chen NK. Correction for eddy current-induced echo-shifting effect in partial-Fourier diffusion tensor imaging. Biomed Res Int 2015;2015:185026.
21. Haselgrove JC, Moore JR. Correction for distortion of echo-planar images used to calculate the apparent diffusion coefficient. Magn Reson Med 1996;36:960–964.
22. Jones DK, Cercignani M. Twenty-five pitfalls in the analysis of diffusion MRI data. NMR Biomed 2010;23:803–820.
23. Meier C, Zwanger M, Feiweier T, Porter D. Concomitant field terms for asymmetric gradient coils: consequences for diffusion, flow, and echo-planar imaging. Magn Reson Med 2008;60:128–134.

SUPPORTING INFORMATION

Additional Supporting Information may be found in the online version of this article.

Video S1. (**a**) Movie cycling through diffusion-weighted images with different diffusion-encoding directions from each technique, (**b**) reconstructed FA maps, and (**c**) FA-weighted primary eigenvector maps, in which the *x, y*, and *z* vector components are mapped to red, green and blue, respectively. The MONO diffusion encoding leads to substantial direction-dependent eddy current image distortions that lead to misregistration between DWI, resulting in regions of artificially high FA. These image distortions (and high FA regions) are reduced with CODE and further reduced with TRSE and EN-CODE.